Proceedings of the ASME 2022 International Technical Conference and Exhibition on Packaging and Integration of Electronic and Photonic Microsystems
InterPACK2022
October 25-27, 2022, Garden Grove, California

IPACK2022-98800

EXPERIMENTAL PROBING OF THE BIAS DEPENDENT SELF-HEATING IN ALGAN/GAN HEMTS WITH A TRANSPARENT INDIUM TIN OXIDE GATE

Anwarul Karim
The Pennsylvania State University
University Park, PA

Tae Kyoung Kim
Korea Institute of Energy Technology
Naju-si, Korea

Daniel Shoemaker
The Pennsylvania State University
University Park, PA

Yiwen Song
The Pennsylvania State University
University Park, PA

Joon Seop Kwak
Korea Institute of Energy Technology
Naju-si, Korea

Sukwon Choi
The Pennsylvania State University
University Park, PA

ABSTRACT

The demand for high power and high-frequency radio frequency (RF) power amplifiers makes AlGaN/GaN high electron mobility transistors (HEMTs) an attractive option due to their large critical field, high saturation velocity, and reduced device footprint as compared to Si-based counterparts. However, due to the high operating power densities, intense device self-heating occurs, which degrades the electrical performance and compromises the device's reliability. The self-heating behavior of AlGaN/GaN HEMTs is known to be not solely a function of the dissipated power but is highly bias-dependent. As the operation of RF power amplifiers involves alteration of the device operation from fully-open to pinched-off channel conditions, it is critical to experimentally map the full channel temperature profile as a function of bias conditions. However, such measurement is difficult using optical thermography techniques due to the lack of optical access underneath the gate electrode, where the peak temperature is expected to occur.

To address this challenge, an AlGaN/GaN HEMT employing a transparent gate made of indium tin oxide (ITO) was fabricated, which enables full channel temperature mapping using Raman spectroscopy. It was found that the maximum channel temperature rise under a partially pinched-off condition is more than ~93% higher than that for an open channel condition, although both conditions would lead to an identical power dissipation level. The channel peak temperature probed in an ITO-gated device (underneath the gate) is ~33% higher than the highest channel temperature that can be measured for a standard metal-gated AlGaN/GaN HEMT (i.e., next to the metal gate structure) operating under an identical bias condition. This indicates that one may significantly underestimate the device's thermal resistance when solely relying on performing thermal characterization on the optically accessible region of a standard AlGaN/GaN HEMT. The outcomes of this study are important in terms of conducting a more accurate lifetime prediction of the device lifetime and designing thermal management solutions.

Keywords: ITO gate, gallium nitride, HEMT, Raman thermometry, peak temperature, thermal reliability, lifetime prediction

NOMENCLATURE

ITO	Indium tin oxide
GaN	Gallium nitride
HEMT	High electron mobility transistor
2DEG	Two-dimensional electron gas
V_{DS}	Drain-source voltage
V_{GS}	Gate-source voltage
I_{DS}	Drain-source current
I_{GS}	Gate-source current
P	Power dissipation

1. INTRODUCTION

AlGaN/GaN high electron mobility transistors (HEMTs) have emerged as an attractive candidate for next-generation high power and high-frequency RF applications due to the exclusive properties of GaN such as the wide bandgap (~3.4 eV), large critical breakdown voltage (~3 MV/cm), and high saturation velocity (~3×10^7 cm/s) [1–3]. Additionally, the formation of a 2-dimensional electron gas (2DEG) near the AlGaN/GaN interface (without intentional doping) provides low ON resistance and high mobility [4]. Besides, these devices offer means to accomplish improved size, weight, and power (SWaP) at the

system level [5], which will benefit 5G communication, broadband satellite, and military radar applications [6–8].

As AlGaN/GaN HEMTs operate at extremely high-power densities [5], the internal heat generation within the 2DEG can drastically increase the channel temperature and cause device degradation [9–11]. Under high voltage operation, an electric field spike develops underneath the drain side corner of the transistor gate [12,13], leading to a non-uniform temperature distribution across the transistor channel and forming a local nanoscale hotspot. If not appropriately cooled, this local hotspot can deteriorate the device's performance and reliability [10,12,14–19]. For example, the device's electrical performance (i.e. output power) was shown to degrade with temperature rise by 0.01 $dB°C^{-1}$ [20]. Intense device self-heating can also affect the device reliability since the mean-time-to-failure (MTTF) reduces by an order of magnitude with a channel temperature rise of ~10 °C [21].

The device self-heating has been reported not to be solely a function of dissipated power but also affected by the operational bias conditions (i.e., the combination of gate-to-source voltage, V_{GS}, and drain-to-source voltage, V_{DS}, applied to a device) [13,17,22,23]. Under RF operation, the device experiences a wide range of biasing from a fully open to a pinched-off channel condition [24,25]. Due to the rapid bias switching under RF operation, a varying level of peak temperature occurs along the device channel [26,27]. Depending on the bias conditions, the Joule heating profile within the device channel is altered [13]. Among the various bias conditions, a fully-open channel condition (under the application of a positive V_{GS} for normally-ON devices) results in a relatively uniform Joule heat distribution across the device channel. On the other hand, under a partially pinched-off condition (under the application of a negative V_{GS}) there develops a local depletion region underneath the drain side corner of the gate, which leads to local confinement of the Joule heating region at this location. Therefore, accurate experimental probing of the channel temperature distribution under various bias conditions is crucial for understanding the self-heating behavior of AlGaN/GaN HEMTs.

To assess the temperature rise in AlGaN/GaN HEMTs, a variety of noninvasive, noncontact optical approaches have been developed. These techniques include infrared (IR) thermal imaging, thermoreflectance thermal imaging (TTI), and Raman thermometry [28–31]. Because of the different operating principles, each technique differs in terms of material selectivity, probing depth, and spatial resolution. IR thermography significantly underestimates the channel temperature because GaN is transparent to IR thermal radiation and the spatial resolution of this method is relatively low [28,30,32,33]. TTI leverages the temperature dependence of the reflectivity of the material surface to be measured [28,29,34]. This technique provides high spatial resolution (~ 0.6 μm) and is most suitable for measuring the temperature of metal electrodes. However, it does not provide means to measure the temperature of materials/layers underneath the device surface. The working principle of Raman thermometry is based on Raman scattering, i.e., the inelastic scattering of photons due to absorption (anti-Stokes Raman scattering) or emission (Stokes Raman scattering) of energy from or to the lattice, respectively [28,35]. This method utilizes a laser excitation source to probe the frequency or energy of phonons (i.e., quantized lattice vibration), allowing indirect measurement of the temperature of the crystalline solids. In general, Raman thermometry measures the surface or depth-averaged temperature of a semiconductor (depending on the bandgap energy of the material) with a spatial resolution of ~1 μm. Standard Raman thermometry can measure the temperature of semiconductors and insulators, but not metals. Unfortunately, none of these optical thermography techniques can map the temperature of the entire channel of a standard AlGaN/GaN HEMT and identify the hotspot due to limited optical access, hindered by the metal gate electrode. The combined use of TTI and nanoparticle-assisted Raman thermometry was demonstrated to measure both the surface temperatures of the metal gate and the channel; however, the channel region underneath the gate was inaccessible [29,30,36,37]. Cross-sectional thermal mapping of an AlGaN/GaN HEMT was reported using TTI [38]. While this approach first allowed optical probing of the hotspot underneath the gate electrode, it is a destructive approach that may alter the device electrical output characteristics. To this day, direct temperature mapping on an as-fabricated AlGaN/GaN HEMT has not been reported in the literature.

AlGaN/GaN HEMTs with an optically transparent gate electrode offers the means to perform nondestructive *in situ* full channel temperature mapping of an operational device. The transparent gate will allow to directly probe the channel temperature underneath the gate using Raman thermometry. A transparent conducting oxide, indium tin oxide (ITO), has been used to construct the Schottky gate electrode of AlGaN/GaN HEMTs [39–42]. Due to its optical transparency, ITO has been used in GaAs transistors as well as GaN light-emitting diodes (LEDs) [43,44]. AlGaN/GaN HEMTs with an ITO-based transparent gate electrode have been previously studied to probe trapping and hot electron effects [39,40] and to enhance the UV detection capability [41]. A thermal reliability study of normally-OFF AlGaN/GaN HEMTs adopting an ITO gate qualitatively showed the degradation of the gate using electro-luminescence (EL) imaging [42].

In this work, an AlGaN/GaN HEMTs with a transparent ITO gate was fabricated and used to fully map the channel temperature, including the channel region underneath the gate, via Raman thermometry. Standard AlGaN/GaN HEMTs with similar device geometry adopting a metal gate electrode were also fabricated and characterized for comparison. Moreover, to better understand the bias-dependent self-heating effect in AlGaN/GaN HEMTs, the ITO-gated device was tested under diverse operating conditions, and the subsequent alteration of the channel temperature distribution was investigated.

2. EXPERIMENTAL METHODS

Two series of AlGaN/GaN HEMTs were fabricated: one set with standard metal (Ni/Au) gates and another set with

transparent ITO gates. Both series assumed similar device dimensions and were fabricated on a commercial GaN-on-Si epitaxial material stack (Figure 1). Thermal characterization was performed on both types of devices using standard Raman thermometry.

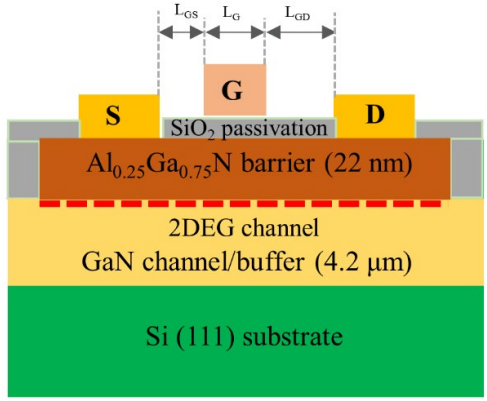

(a)

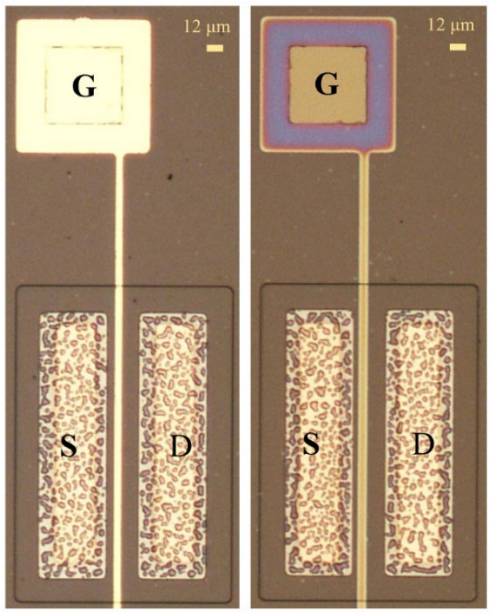

(b)

FIGURE 1: (a) CROSS-SECTIONAL SCHEMATIC OF THE AlGaN/GaN HEMTS, AND (b) OPTICAL IMAGES OF DEVICES WITH A METAL GATE (LEFT) AND AN ITO GATE (RIGHT).

2.1 Device description

The AlGaN/GaN HEMTs were fabricated on a GaN-on-Si wafer. A 4.2 µm thick GaN channel/buffer layer is grown on a 1000 µm thick Si substrate (with a transition interlayer). A 22 nm thick $Al_{0.25}Ga_{0.75}N$ barrier layer is grown on the GaN channel to form 2-dimensional electron gas (2DEG). The Ohmic contacts are formed by e-beam evaporation of a Ti/Al/Ni/Au (20/80/50/50 nm) metal stack, followed by rapid thermal annealing (RTA) at 850 ºC for 1 minute. 350 nm-deep inductively-coupled-plasma (ICP) etching is performed to achieve mesa isolation before forming the Ohmic contacts. A 100 nm thick SiO_2 passivation layer is deposited by sputtering. For the metal-gated AlGaN/GaN HEMTs, a Ni/Au (50/100 nm) Schottky gate is constructed using e-beam evaporation. For AlGaN/GaN HEMTs with transparent gates, 150 nm thick ITO is sputtered, followed by RTA at 600 ºC for 1 minute. Both metal and nonmetal (ITO) gate AlGaN/GaN HEMTs possess similar device structures and dimensions. The gate length (L_G) is 5 µm and the channel width is 170 µm. An identical mask layout was used during device fabrication; however, there is a slight difference in the L_{GD} of the fabricated ITO- and metal-gated HEMTs. The measured L_{GD} of the ITO-gated HEMT is 15.8 µm, whereas it is 16.6 µm for metal-gated HEMT. The epitaxial structure and optical images of the devices are shown in Figure 1(a) and (b), respectively.

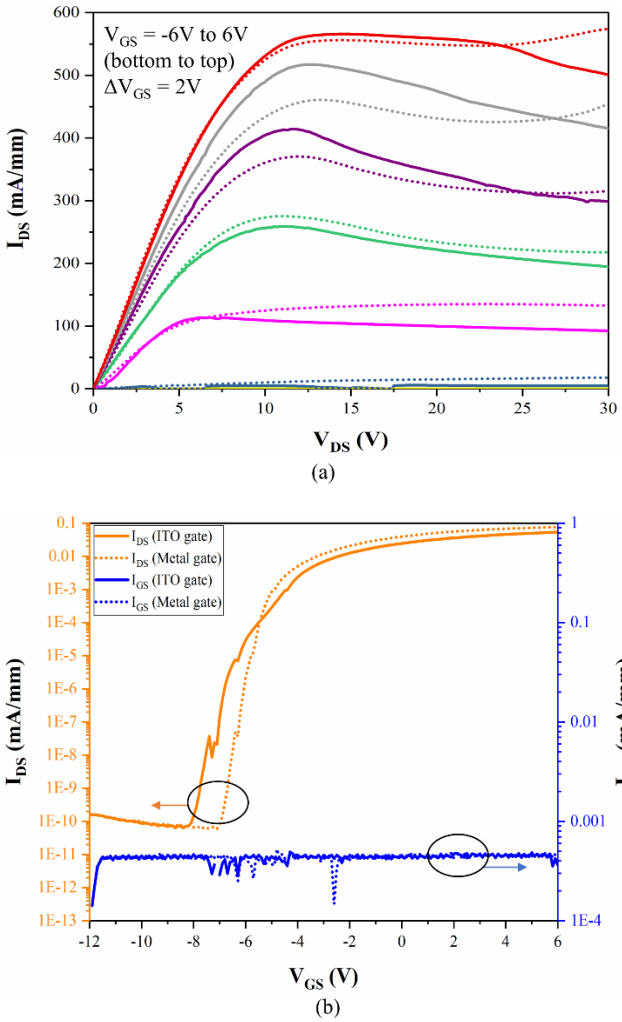

FIGURE 2: (a) DEVICE OUTPUT CHARACTERISTICS AND (b) TRANSFER CHARACTERISTICS. DOTTED LINES ARE FOR THE METAL-GATED HEMT AND SOLID LINES ARE FOR THE ITO GATE HEMT.

The electrical output (I_{DS}-V_{DS}) and transfer (I_{DS}-V_{GS}) characteristics of the metal- and ITO-gated HEMTs are shown in

Figure 2. Both devices were tested under identical voltage bias sweeping (V_{GS}: from -12V to 6V; V_{DS}: from 0V to 30V). The output characteristics in Figure 2(a) show that for all V_{GS} conditions, the drain currents (I_{DS}) for the two device structures in the linear region are almost identical. Notable self-heating is observed in both devices at higher V_{DS} conditions as I_{DS} drops after reaching the saturation region (Figure 2(a)). The decrease in I_{DS} is slightly more prominent for the ITO-gated HEMT compared to metal gate HEMT, which may be due to the slight difference in the gate-to-source (L_{GD}) spacings of the two device structures and/or the lower thermal conductivity of ITO than gold. A higher channel temperature results in a reduced carrier (i.e. electron) mobility as a consequence of increased electron-phonon scattering rates [7,8]. From the transfer characteristics shown in Figure 2(b), the threshold voltages (V_{Th}) at V_{DS} = 10V is obtained as -8V for the ITO-gated HEMT and -7V for the metal-gated HEMT, respectively. The gate leakage current (I_{GS}) is low and similar for both devices.

2.2 Raman thermometry

Raman thermometry is an optical thermography technique that measures the lattice temperature by probing the energy or frequency shift of optical phonons, which can be observed either through anti-Stokes or Stokes Raman scattering. A Raman system consists of an excitation laser, microscope, spectrometer, and detector such as a charge-coupled device (CCD) [35]. Raman scattering is generated by laser excitation of the sample under the microscope. In the spectrometer, the scattered photons are collected, dispersed by a grating, and counted by a CCD. This process provides spectral information on the Raman-active optical phonons, which includes the Raman peak position, intensity, and full-width-at-half-maximum (FWHM). The Raman setup used in this study is shown in Figure 3.

FIGURE 3: PHOTOGRAPH OF THE RAMAN THERMOMETRY SETUP (FL stands for "fluorescent").

Raman thermometry is suitable for characterizing AlGaN/GaN HEMTs due to its relatively high spatial resolution (<1 μm) and lenience to device operation when using a sub-bandgap laser excitation wavelength [28]. When using such a laser excitation source without any surface temperature transducer [29,45,46] deposited on the sample surface, a depth-averaged temperature of the GaN layer is measured [28]. To perform the temperature mapping, a Horiba LabRAM HR Evolution Raman spectrometer equipped with 532 nm laser excitation (2.33eV) was used in this work. A long working distance 50× objective (NA=0.45) was employed in a 180° backscattering configuration for the measurement. This standard Raman thermometry setup offers a spatial resolution of ~600 nm. To improve the signal-to-noise ratio of the measurement results, the Raman system is equipped with an electron-multiplying CCD (EMCCD). The laser power was carefully controlled (~1 mW) to prevent laser-induced heating on the Si substrate [30,47].

Temperature measurement using Raman spectroscopy can be done using the shift in the Raman peak position, change in the linewidth, and the anti-Stokes to Stokes intensity ratio [35]. For AlGaN/GaN HEMTs, a multi-spectral method that takes advantage of fitting two Raman peaks is most widely used [48]. This is because the Raman peak position is not only influenced by the lattice temperature rise but also the evolution of mechanical stress [35]. During device operation, a temperature gradient forms in response to Joule heating, which results in operational thermo-elastic stress in the GaN layer. In addition, inverse piezoelectric stress forms in GaN in response to the internal vertical electric field [17]. For accurate temperature measurement, the contribution from these mechanical stress effects must be separated from the overall shift in the Raman peak positions. The two-peak fit method [48] can be employed to measure the lattice temperature rise (ΔT) independent of mechanical stress effects, with lower uncertainty than linewidth and anti-Stokes to Stokes intensity ratio-based methods [35]. Moreover, this method does not require a temperature calibration process to determine the temperature rise in GaN thin films [48]. Therefore, the two-peak fit method was used in this study, and the relevant temperature and biaxial stress conversion coefficients were adopted from the reference [48] to map the GaN layer temperature of the devices. To calculate ΔT, first, the fully pinched-off condition (V_{GS} = -12V; same V_{DS} as ON-state conditions are applied for each measurement) is taken as a reference. Second, Raman measurements are taken during open channel and/or partially pinched-off conditions where the device dissipates power. Finally, the difference in the E_2(high) and A_1(LO) Raman peak positions are processed according to procedures listed in reference [48] to derive the ΔT.

3. RESULTS AND DISCUSSION

A comparison of the measured channel temperature maps of the metal- and ITO-gated AlGaN/GaN HEMTs are illustrated in Figure 4 for open channel and partially pinched-off conditions that lead to an identical power dissipation level of 500 mW. Under an open channel condition of V_{GS} = 6V, V_{DS} ~ 6V (adjusted to accomplish the same P for both devices), and P = 500 mW (Figure 4 (a)), the temperature distribution is relatively uniform across the entire channel for the ITO-gated device. The optically accessible channel region of a metal-gated HEMT also

does not show a sharp temperature gradient. Under such open channel conditions, charge carriers (i.e., electrons) traversing across the source and drain electrodes encounter a relatively uniform electrical resistance across the entire channel. A nearly linear voltage drop occurs along the channel length; hence, heat is generated almost uniformly across the entire channel. Under identical power conditions, the channel temperature of the ITO-gated HEMT is slightly higher than that of the metal-gated HEMT, which is consistent with the relatively larger current droop observed in its I-V characteristics (for the saturation region at high power dissipation levels) shown in Figure 2(a). Again, this is thought to be caused by the slight difference in the gate-to-drain spacings of the two device structures and/or the lower thermal conductivity of ITO (for the ITO gate) than gold (for the metal gate which is mostly comprised of gold). Larger uncertainties in temperature data underneath the ITO gate region (channel locations of 3.5, 6, and 8.5 μm from the source electrode) observed in Figure 4(a) are caused by the lower signal intensity of the GaN Raman peak as compared to those acquired from the rest of the channel.

Figure 4(b) shows the channel temperature distributions of the two AlGaN/GaN HEMTs under a partially pinched-off condition of V_{GS} = -2V, V_{DS} ~ 15V (adjusted to accomplish the same P for both devices), and P = 500 mW (full channel pinched-off occurs at $V_{GS} \leq$ -7V). When a negative gate bias is applied, the charge carrier density reduces underneath the drain-side corner of the gate, i.e., a local depletion region is formed [8]. This local region, where the electrical resistance is higher than the rest of the channel, leads to Joule heat concentration. The Raman temperature map depicts a sharp temperature rise underneath the ITO gate on the drain side of the device. The channel peak temperature is not observable by characterizing a metal-gated device due to the lack of optical access underneath the gate electrode. As shown in Figure 4(b), the maximum temperature measured underneath the ITO gate is ~106°C, whereas the temperature next to the ITO gate (drain side) is ~88°C, which is a ~17 % lower value. This indicates that the highest channel temperature measured from a standard metal-gated HEMT (at a location next to the drain side of the gate) will underestimate the true channel peak temperature. Moreover, the exact location prone to device degradation (where the electric field strength and temperature are highest) remains inaccessible when characterizing a metal-gated HEMT. Therefore, a transparent ITO-gated device can provide effective means to perform thermal reliability studies and lifetime estimation.

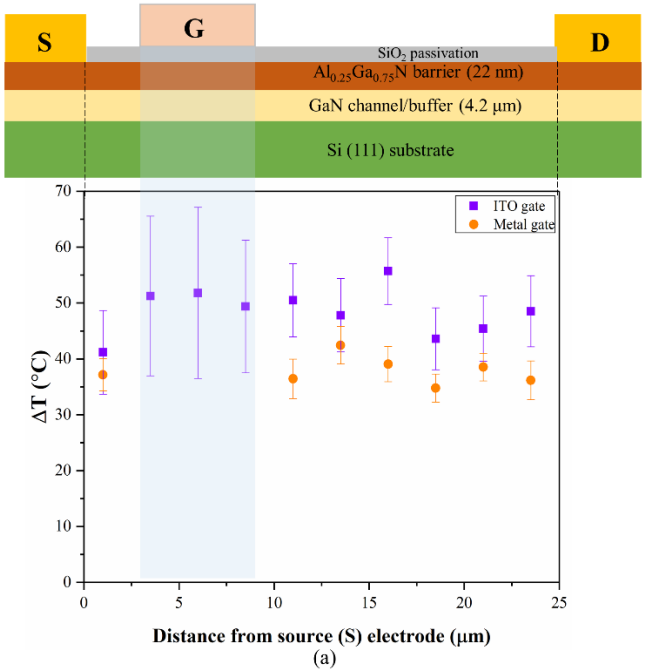

FIGURE 4: COMPARISON OF FULL CHANNEL TEMPERATURE MAPS FOR THE ITO-AND METAL-GATED AlGaN/GaN HEMTS AT A POWER DISSIPATION LEVEL OF 500 mW FOR (a) AN OPEN CHANNEL CONDITION AND (b) A PARTIALLY PINCHED-OFF CONDITION.

Experimental observations of the ITO-gated AlGaN/GaN HEMT suggest that the device reliability and lifetime will be significantly impacted by the bias-dependent self-heating behavior. For the same device (i.e., ITO-gated HEMT), the maximum channel temperature occurring under an open channel condition is ~55 ° C, whereas the value for a partially pinched-

off condition is ~106 ºC (~93% higher), despite both conditions lead to an identical power dissipation level of 500 mW. As shown in Figure 4(b), the channel peak temperature occurs underneath the gate on the drain side during a partially pinched-off condition. Additional measurements were performed to see if this peak temperature would further increase for the same power condition when a larger negative gate bias is applied. Figure 5 shows the full channel temperature map for more aggressively pinched-off bias conditions, such as V_{GS}=-2V/V_{DS}=15V, V_{GS} =-3V/V_{DS}=25V, and V_{GS}=-3.5V/V_{DS}=30V (for all conditions, V_{DS} is adjusted to achieve P = 500 mW). The peak temperature rises at the drain-side underneath the gate are 106.3 ºC, 133.6 ºC, and 141.6 ºC for the respective partially pinched-off conditions. These results indicate that the channel peak temperature increases as bias conditions lead to a more progressively pinched-off channel being applied to the device. This is because, with a larger negative V_{GS} (that entails a higher V_{DS} to attain the same power dissipation level), the depletion region extends further down towards the GaN layer at the drain side of the gate and shrinks in size along the channel length. This further restricts charge carrier flow across the channel and concentrates the Joule heating, eventually leading to an increase in the channel peak temperature [13].

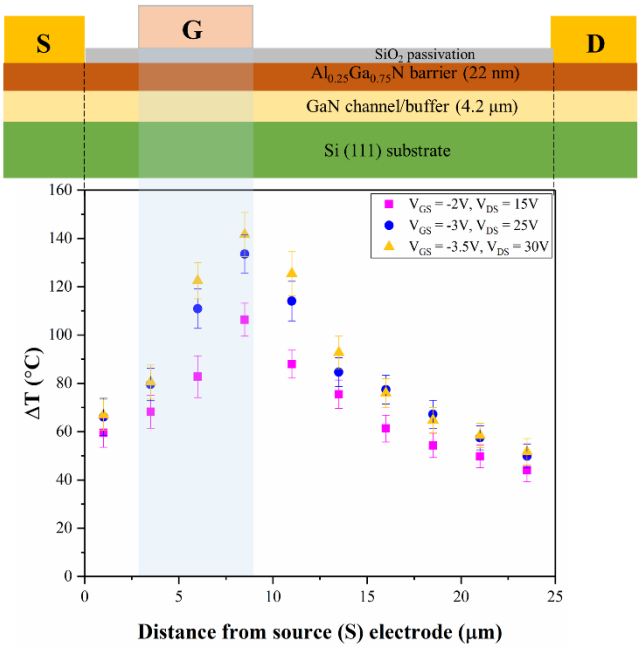

FIGURE 5: FULL CHANNEL TEMPERATURE MAP OF THE ITO-GATED AlGaN/GaN HEMTS AT 500 mW POWER DISSIPATION FOR VARIOUS PARTIALLY PINCHED-OFF CONDITIONS.

4. CONCLUSION

This experimental study, for the first time, demonstrates direct measurement of the full channel temperature distribution of an AlGaN/GaN HEMT and identifies the location where the peak channel temperature occurs using a transparent ITO-gated HEMT. The comparison between a standard HEMT with a metal gate and a transparent ITO gate suggests that solely relying upon optical probing of a conventional metal-gated HEMT may result in a significant underestimation of the channel peak temperature. This could lead to overprediction of the device lifetime and inaccurate reliability analysis. It should be noted that, even though the present study provides a more accurate peak temperature estimation than existing studies using conventional device structures, the actual peak temperature occurring in the 2DEG region will be higher than data acquired from Raman thermometry. The temperatures determined by Raman thermometry represent a depth-averaged value within a ~1 µm laser spot through the thickness of the GaN layer. Our future work will focus on calculating the actual device peak temperature using a coupled electro-thermal device model [22,23,49,50] that is calibrated against Raman results obtained in this work.

ACKNOWLEDGEMENTS

This work was supported by the National Science Foundation under Grant No. CBET-1934482 (Program Director: Ying Sun). This work was also supported by the KENTECH Research (Grant No. KRG2021-01-002).

REFERENCES

[1] Pengelly, R. S., Wood, S. M., Milligan, J. W., Sheppard, S. T., and Pribble, W. L., 2012, "A Review of GaN on SiC High Electron-Mobility Power Transistors and MMICs," IEEE Trans. Microw. Theory Tech., **60**(6 PART 2), pp. 1764–1783.

[2] Mishra, U. K., Parikh, P., and Wu, Y. F., 2002, "AlGaN/GaN HEMTs - An Overview of Device Operation and Applications," Proc. IEEE, **90**(6), pp. 1022–1031.

[3] Shur, M. S., 1998, "GaN Based Transistors for High Power Applications," Solid. State. Electron., **42**(12), pp. 2131–2138.

[4] Ambacher, O., Foutz, B., Smart, J., Shealy, J. R., Weimann, N. G., Chu, K., Murphy, M., Sierakowski, A. J., Schaff, W. J., Eastman, L. F., Dimitrov, R., Mitchell, A., and Stutzmann, M., 1999, "Two Dimensional Electron Gases Induced by Spontaneous and Piezoelectric Polarization in Undoped and Doped AlGaN/GaN Heterostructures," J. Appl. Phys., **87**(1), p. 334.

[5] Bar-Cohen, A., Maurer, J. J., and Altman, D. H., 2019, "Embedded Cooling for Wide Bandgap Power Amplifiers: A Review," J. Electron. Packag. Trans. ASME, **141**(4).

[6] Mishra, U. K., Shen, L., Kazior, T. E., and Wu, Y. F., 2008, "GaN-Based RF Power Devices and Amplifiers," Proc. IEEE, **96**(2), pp. 287–305.

[7] Wu, Y. F., Keller, B. P., Keller, S., Kapolnek, D., Kozodoy, P., Denbaars, S. P., and Mishra, U. K., 1997, "High Power AlGaN/GaN HEMTs for Microwave

Applications," Solid. State. Electron., **41**(10), pp. 1569–1574.
[8] Trew, R. J., Bilbro, G. L., Kuang, W., Liu, Y., and Yin, H., 2005, "Microwave AlGaN/GaN HFETs," IEEE Microw. Mag., **6**(1), pp. 56–66.
[9] McAlister, S. P., Bardwell, J. A., Haffouz, S., and Tang, H., 2006, "Self-Heating and the Temperature Dependence of the Dc Characteristics of GaN Heterostructure Field Effect Transistors," J. Vac. Sci. Technol. A Vacuum, Surfaces, Film., **24**(3), p. 624.
[10] Meneghesso, G., Verzellesi, G., Danesin, F., Rampazzo, F., Zanon, F., Tazzoli, A., Meneghini, M., and Zanoni, E., 2008, "Reliability of GaN High-Electron-Mobility Transistors: State of the Art and Perspectives," IEEE Trans. Device Mater. Reliab., **8**(2), pp. 332–343.
[11] Chou, Y. C., Leung, D., Smorchkova, I., Wojtowicz, M., Grundbacher, R., Callejo, L., Kan, Q., Lai, R., Liu, P. H., Eng, D., and Oki, A., 2004, "Degradation of AlGaN/GaN HEMTs under Elevated Temperature Lifetesting," Microelectron. Reliab., **44**(7), pp. 1033–1038.
[12] Heller, E., Choi, S., Dorsey, D., Vetury, R., and Graham, S., 2013, "Electrical and Structural Dependence of Operating Temperature of AlGaN/GaN HEMTs," Microelectron. Reliab., **53**(6), pp. 872–877.
[13] Choi, S., Heller, E. R., Dorsey, D., Vetury, R., and Graham, S., 2013, "The Impact of Bias Conditions on Self-Heating in AlGaN/GaN HEMTs," IEEE Trans. Electron Devices, **60**(1), pp. 159–162.
[14] Benbakhti, B., Soltani, A., Kalna, K., Rousseau, M., and De Jaeger, J. C., 2009, "Effects of Self-Heating on Performance Degradation in AlGaN/GaN-Based Devices," IEEE Trans. Electron Devices, **56**(10), pp. 2178–2185.
[15] Liang, M., and Law, M. E., 1994, "Influence of Lattice Self-Heating and Hot-Carrier Transport on Device Performance," IEEE Trans. Electron Devices, **41**(12), pp. 2391–2398.
[16] Wang, X. D., Hu, W. Da, Chen, X. S., and Lu, W., 2012, "The Study of Self-Heating and Hot-Electron Effects for AlGaN/GaN Double-Channel HEMTs," IEEE Trans. Electron Devices, **59**(5), pp. 1393–1401.
[17] Choi, S., Heller, E., Dorsey, D., Vetury, R., and Graham, S., 2013, "The Impact of Mechanical Stress on the Degradation of AlGaN/GaN High Electron Mobility Transistors," J. Appl. Phys., **114**(16), p. 164501.
[18] Hosch, M., Pomeroy, J. W., Sarua, A., Kuball, M., Jung, H., and Schumacher, H., "Field Dependent Self-Heating Effects in High-Power AlGaN/GaN HEMTs."
[19] Nuttinck, S., Gebara, E., Laskar, J., and Harris, H. M., 2001, "Study of Self-Heating Effects, Temperature-Dependent Modeling, and Pulsed Load-Pull Measurements on GaN HEMTs," IEEE Trans. Microw. Theory Tech., **49**(12), pp. 2413–2420.
[20] Ditri, J., Pearson, R. R., Cadotte, R., Hahn, J. W., Fetterolf, D., McNulty, M., and Luppa, D., 2016, "GaN Unleashed: The Benefits of Microfluidic Cooling," IEEE Trans. Semicond. Manuf., **29**(4), pp. 376–383.
[21] Green, D. S., Brown, J. D., Vetury, R., Lee, S., Gibb, S. R., Krishnamurthy, K., Poulton, M. J., Martin, J., and Shealy, J. B., 2008, "Status of GaN HEMT Performance and Reliability," Gall. Nitride Mater. Devices III, **6894**, p. 68941M.
[22] Chatterjee, B., Dundar, C., Beechem, T. E., Heller, E., Kendig, D., Kim, H., Donmezer, N., and Choi, S., 2020, "Nanoscale Electro-Thermal Interactions in AlGaN/GaN High Electron Mobility Transistors," J. Appl. Phys., **127**(4), p. 044502.
[23] Pearson, R., Chatterjee, B., Kim, S., Graham, S., Rattner, A., and Choi, S., 2020, "Guidelines for Reduced-Order Thermal Modeling of Multifinger GaN HEMTs," J. Electron. Packag. Trans. ASME, **142**(2).
[24] Burnham Shawn D, and Paine Bruce M., 2017, "(PDF) Towards an RF GaN Reliability Standard," *JEDEC Reliability of Compound Semiconductors Workshop (ROCS*, JEDEC , Indian Wells, CA, USA.
[25] Camarchia, V., Cappelluti, F., Pirola, M., Guerrieri, S. D., and Ghione, G., 2007, "Self-Consistent Electrothermal Modeling of Class A, AB, and B Power GaN HEMTs under Modulated RF Excitation," IEEE Trans. Microw. Theory Tech., **55**(9), pp. 1824–1831.
[26] Pavlidis, G., Som, S., Barrett, J., Struble, W., and Graham, S., 2019, "The Impact of Temperature on GaN/Si HEMTs under RF Operation Using Gate Resistance Thermometry," IEEE Trans. Electron Devices, **66**(1), pp. 330–336.
[27] Pomeroy, J. W., Uren, M. J., Lambert, B., and Kuball, M., 2015, "Operating Channel Temperature in GaN HEMTs: DC versus RF Accelerated Life Testing," Microelectron. Reliab., **55**(12), pp. 2505–2510.
[28] Oh, S. K., Lundh, J. S., Shervin, S., Chatterjee, B., Lee, D. K., Choi, S., Kwak, J. S., and Ryou, J. H., 2019, "Thermal Management and Characterization of High-Power Wide-Bandgap Semiconductor Electronic and Photonic Devices in Automotive Applications," J. Electron. Packag. Trans. ASME, **141**(2).
[29] Lundh, J. S., Song, Y., Chatterjee, B., Baca, A. G., Kaplar, R. J., Armstrong, A. M., Allerman, A. A., Klein, B. A., Kendig, D., Kim, H., and Choi, S., 2020, "Device-Level Multidimensional Thermal Dynamics with Implications for Current and Future Wide Bandgap Electronics," J. Electron. Packag. Trans. ASME, **142**(3).
[30] Lundh, J. S., Chatterjee, B., Dallas, J., Kim, H., and Choi, S., 2017, "Integrated Temperature Mapping of Lateral Gallium Nitride Electronics," Proc. 16th Intersoc. Conf. Therm. Thermomechanical Phenom. Electron. Syst. ITherm 2017, pp. 320–327.
[31] Kuball, M., and Pomeroy, J. W., 2016, "A Review of Raman Thermography for Electronic and Opto-Electronic Device Measurement with Submicron Spatial and Nanosecond Temporal Resolution," IEEE Trans. Device Mater. Reliab., **16**(4), pp. 667–684.
[32] Killat, N., Kuball, M., Chou, T. M., Chowdhury, U., and

Jimenez, J., 2010, "Temperature Assessment of AlGaN/GaN HEMTs: A Comparative Study by Raman, Electrical and IR Thermography," IEEE Int. Reliab. Phys. Symp. Proc., pp. 528–531.

[33] Choi, S., Peake, G. M., Keeler, G. A., Geib, K. M., Briggs, R. D., Beechem, T. E., Shaffer, R. A., Clevenger, J., Patrizi, G. A., Klem, J. F., Tauke-Pedretti, A., and Nordquist, C. D., 2016, "Thermal Design and Characterization of Heterogeneously Integrated InGaP/GaAs HBTs," IEEE Trans. Components, Packag. Manuf. Technol., **6**(5), pp. 740–748.

[34] Maize, K., Heller, E., Dorsey, D., and Shakouri, A., 2012, "Thermoreflectance CCD Imaging of Self Heating in AlGaN/GaN High Electron Mobility Power Transistors at High Drain Voltage," Annu. IEEE Semicond. Therm. Meas. Manag. Symp., pp. 173–181.

[35] Beechem, T., Christensen, A., Graham, S., and Green, D., 2008, "Micro-Raman Thermometry in the Presence of Complex Stresses in GaN Devices," J. Appl. Phys., **103**(12), p. 124501.

[36] Chatterjee, B., Armstrong, A. M., Klein, B. A., Bansal, A., Seyf, H. R., Talreja, D., Pogrebnyakov, A., Heller, E., Gopalan, V., Henry, A. S., Redwing, J. M., Lundh, J. S., Foley, B., Choi, S., Song, Y., Shoemaker, D., Baca, A. G., Kaplar, R. J., Beechem, T. E., Saltonstall, C., and Allerman, A. A., 2020, "Interdependence of Electronic and Thermal Transport in AlxGa1-XN Channel HEMTs," IEEE Electron Device Lett., **41**(3), pp. 461–464.

[37] Lundh, J. S., Chatterjee, B., Song, Y., Baca, A. G., Kaplar, R. J., Beechem, T. E., Allerman, A. A., Armstrong, A. M., Klein, B. A., Bansal, A., Talreja, D., Pogrebnyakov, A., Heller, E., Gopalan, V., Redwing, J. M., Foley, B. M., and Choi, S., 2019, "Multidimensional Thermal Analysis of an Ultrawide Bandgap AlGaN Channel High Electron Mobility Transistor," Appl. Phys. Lett., **115**(15), p. 153503.

[38] Pavlidis, G., Hilton, A. M., Brown, J. L., Heller, E. R., and Graham, S., 2020, "Monitoring the Joule Heating Profile of GaN/SiC High Electron Mobility Transistors via Cross-Sectional Thermal Imaging," J. Appl. Phys., **128**(7), p. 075705.

[39] Pei, Y., Vampola, K. J., Chen, Z., Chu, R., DenBaars, S. P., and Mishra, U. K., 2009, "AlGaN/GaN HEMT with a Transparent Gate Electrode," IEEE Electron Device Lett., **30**(5), pp. 439–441.

[40] Meneghini, M., Ronchi, N., Stocco, A., Meneghesso, G., Mishra, U. K., Pei, Y., and Zanoni, E., 2011, "Investigation of Trapping and Hot-Electron Effects in GaN HEMTs by Means of a Combined Electrooptical Method," IEEE Trans. Electron Devices, **58**(9), pp. 2996–3003.

[41] Narita, T., Wakejima, A., and Egawa, T., 2013, "Ultraviolet Photodetectors Using Transparent Gate AlGaN/GaN High Electron Mobility Transistor on Silicon Substrate," Jpn. J. Appl. Phys., **52**(1 PART2), p. 01AG06.

[42] Lu, Y., Li, B., Tang, X., Jiang, Q., Yang, S., Tang, Z., and Chen, K. J., 2015, "Normally off Al2O3-AlGaN/GaN MIS-HEMT with Transparent Gate Electrode for Gate Degradation Investigation," IEEE Trans. Electron Devices, **62**(3), pp. 821–827.

[43] Li, W. Q., Karakucuk, M., Kulman, J., East, J. R., Haddad, G. I., and Bhattacharya, P. K., 1993, "High Frequency GaAs/Al0.25Ga0.75As Heterojunction Bipolar Transistors with Transparent Indium-Tin-Oxide Emitter Contacts," Electron. Lett., **29**(25), pp. 2223–2225.

[44] Narukawa, Y., Sano, M., Sakamoto, T., Yamada, T., and Mukai, T., 2008, "Successful Fabrication of White Light Emitting Diodes by Using Extremely High External Quantum Efficiency Blue Chips," Phys. status solidi, **205**(5), pp. 1081–1085.

[45] Lundh, J. S., Zhang, T., Zhang, Y., Xia, Z., Wetherington, M., Lei, Y., Kahn, E., Rajan, S., Terrones, M., and Choi, S., 2020, "2D Materials for Universal Thermal Imaging of Micro- and Nanodevices: An Application to Gallium Oxide Electronics," ACS Appl. Electron. Mater., **2**(9), pp. 2945–2953.

[46] Dallas, J., Pavlidis, G., Chatterjee, B., Lundh, J. S., Ji, M., Kim, J., Kao, T., Detchprohm, T., Dupuis, R. D., Shen, S., Graham, S., and Choi, S., 2018, "Thermal Characterization of Gallium Nitride P-i-n Diodes," Appl. Phys. Lett., **112**(7), p. 073503.

[47] Chatterjee, B., Shoemaker, D., Song, Y., Shi, T., Huang, H. L., Keum, D., Krishnan, A., Foley, B. M., Jovanovic, I., Hwang, J., Kim, H., and Choi, S., 2020, "Cumulative Impacts of Proton Irradiation on the Self-Heating of AlGaN/GaN HEMTs," ACS Appl. Electron. Mater., **2**(4), pp. 980–991.

[48] Choi, S., Heller, E. R., Dorsey, D., Vetury, R., and Graham, S., 2013, "Thermometry of AlGaN/GaN HEMTs Using Multispectral Raman Features," IEEE Trans. Electron Devices, **60**(6), pp. 1898–1904.

[49] Chatterjee, B., Lundh, J. S., Dallas, J., Kim, H., and Choi, S., 2017, "Electro-Thermal Reliability Study of GaN High Electron Mobility Transistors," Proc. 16th Intersoc. Conf. Therm. Thermomechanical Phenom. Electron. Syst. ITherm 2017, pp. 1247–1252.

[50] Tadjer, M., and Anderson, T., 2022, *Thermal Management of Gallium Nitride Electronics*, Elsevier Science.

